Structural transition and magnetic properties of high Cr-doped $BiFeO_3$ ceramic

(Transição estrutural e propriedades magnéticas da cerâmica $BiFeO_3$ dopada com Cr)

S. S. Arafat[1,2]*

[1]King Faisal University, Faculty of Science, Physics Department, Saudi Arabia

[2]Fayoum University, Faculty of Science, Physics Department, Egypt

Abstract

Magnetic properties of $BiFe_{1-x}Cr_xO_3$ perovskite-type solids reaction synthesized at high pressure were investigated and a magnetic phase diagram was established. X-ray diffraction data revealed a crystal structure transformation from rhombohedral to monoclinic as Cr^{3+} ions substituted Fe ions in the samples. Néel temperature T_N and spin-reorientation temperature T_{SR} were determined from dM/dT by measuring the temperature dependence of magnetization (M-T). The magnetization results indicated that T_N and T_{SR} were strongly dependent on Cr^{3+} ion doping; both T_N and T_{SR} decreased with the increase of Cr^{3+} doping. The magnetic hysteresis loops investigated at room temperature reflected an antiferromagnetic behavior from x= 0.4 to 0.6 and weak ferromagnetic at x=1.0. Besides, the remnant magnetization M_r and maximum magnetization M_{max} increased with increasing x from 0.4 up to 1.0. The Cr doping was found to be helpful in reducing coercivity H_c for the magnetic samples from x= 0.4 to 0.8 and their applications as magnetic sensors are possible.

Keywords: perovskite-type structure, high-pressure solid-state synthesis, X-ray diffraction, magnetic properties.

Resumo

Propriedades magnéticas de $BiFe_{1-x}Cr_xO_3$ do tipo perovskita sintetizado por reação no estado sólido a alta pressão foram investigadas e um diagrama de fase magnética foi estabelecido. Os dados de difração de raios X revelaram a transformação da estrutura cristalina de romboédrica para monoclínica conforme íons de Cr^{3+} substituíram íons de Fe nas amostras. As temperaturas de Néel T_N e de reorientação de spin T_{SR} foram determinadas a partir de dM/dT por meio da medição da magnetização em função da temperatura (M-T). Os resultados da magnetização indicaram que T_N e T_{SR} foram fortemente dependentes da dopagem de íon Cr^{3+}; T_N e T_{SR} diminuíram com o aumento da dopagem de Cr^{3+}. Os laços de histerese magnética investigados à temperatura ambiente refletiram um comportamento antiferromagnético de x= 0,4 a 0,6 e ferromagnético fraco em x=1,0. Além disso, a magnetização remanescente M_r e a magnetização máxima M_{max} aumentaram com o aumento de x de 0,4 até 1,0. A dopagem de Cr foi útil na redução da coercividade H_c para amostras magnéticas de x= 0,4 a 0,8 e suas aplicações como sensores magnéticos são possíveis.

***Palavras-chave**: estrutura perovskita, síntese em estado sólido de alta pressão, difração de raios X, propriedades magnéticas.*

INTRODUCTION

Multiferroics materials possessing coupling of two or more types of ordering like ferromagnetic and ferroelasticity in a single-phase have exposed a lot of interest in physics and opens many possibilities of practical applications in modern technologies. These kinds of materials have been investigated for a new type of memory applications using a combination of ferromagnetic and ferroelectric properties [1-4]. This class of materials has found its applications in the field of electro-optic transducer controlled by magnetism and microwave devices [5]. Moreover, the ferroelectro-magnetic phenomena have long aroused intense interest for researchers in the solid-state and material sciences.

Among the multiferroic materials, $BiFeO_3$ belonging to ABO_3 family with a rhombohedrally distorted simple perovskite structure with a space group R3c has been of much interest due to its relatively high antiferromagnetic-paramagnetic Néel temperature T_N=653-643 K [6, 7] and its ferroelectric-paraelectric Curie temperature, T_C=1103 K [8]. Several studies have been performed to determine the crystal structures and magnetic properties of $BiFeO_3$, encouraged to a great extent by its potential magneto-electric properties [9]. $BiFeO_3$ exhibits antiferromagnetic and ferroelectric order concurrently. The antiferromagnetic order originates from unpaired electrons in the d orbitals of Fe^{3+} ions at the B positions of the perovskite crystal structure [10, 11], while the ferroelectric order is caused by the free electron pair in an s-p hybrid orbital of Bi^{3+} occupying the A site. This antiferromagnetic order can be changed in different ways, one of them by cationic substitution,

**ssoliman@kfu.edu.sa, samia.arafat@yahoo.com*

https://orcid.org/0000-0001-6811-8142

thus leading to a ferromagnetic response [12]. Another perovskite multiferroic material is $BiCrO_3$ which was first synthesized in 1968 by firing under very high pressure. It has a monoclinic C2 structure at room temperature, exhibits a parasitic ferromagnetic ordering at 123 K, and undergoes a structural phase transition at 440 K [13].

The doping process is recognized to be a suitable method to change the specific physical properties of a material [14-19]. The nature of the doping effect has been studied by doping $BiFeO_3$ with Cr. $BiFe_{1-x}Cr_xO_3$ (x=0.4-1.0), where a portion of Fe^{3+} ions is substituted by Cr^{3+} ions, are studied. High-pressure synthesis is a powerful technique to explore new materials. $BiFe_{1-x}Cr_xO_3$ with perovskite-type structure was reported to be synthesized under high pressure of 7 GPa. In this study, the performance of X-ray powder diffraction at room temperature, magnetization characteristics with temperature, and their hysteresis loops at room temperature are conducted.

EXPERIMENTAL

The polycrystalline ceramics samples of $BiFe_{1-x}Cr_xO_3$ (x= 0.4, 0.5, 0.6, 0.8, and 1.0) were prepared by a solid-state reaction technique under a high pressure of 7 GPa. Mixed powders of Bi_2O_3 (99.9%), Fe_2O_3 (99.9%), and Cr_2O_3 (99.9%) with stoichiometric proportion (1:1 molar ratio) were mixed in an agate mortar for 0.5 h. Afterward, these were packed into gold capsules (~4x6 mm^2) and was calcined in a cubic anvil-type apparatus under 7 GPa at 1000 °C for 1 h [20].

X-ray diffraction experiments were carried out using a diffractometer with CuKα source. The X-ray pattern was recorded at an interval of 0.010° at room temperature. The structural parameters were refined by Rietveld analysis of diffraction data in the 2θ range of 20°-65°. The magnetic properties were measured using a superconducting quantum interference device magnetometer (SQUID, Quantum Design). The data were collected under zero-field cooling and field cooling at 1 kOe from 5 to 400 K, below and above the Néel and spin-reorientation temperatures.

RESULTS AND DISCUSSION

Structural analysis: Fig. 1a shows the X-ray powder diffraction (XRD) patterns for $BiFe_{1-x}Cr_xO_3$ where x= 0.4, 0.5, 0.6, 0.8, and 1.0 at room temperature (RT). The patterns revealed that the peaks were sharp and strong indicated a good crystallization aspect of the samples. There were some impurity phases of $BiFeO_9$, Bi_2O_3, and $Bi_{25}FeO_{40}$ formed along with the $BiFeO_3$ phase in the solid-state reaction process, as reported by several authors [21-24]. The percentage of the impurity phases determined by calculating the ratio of the

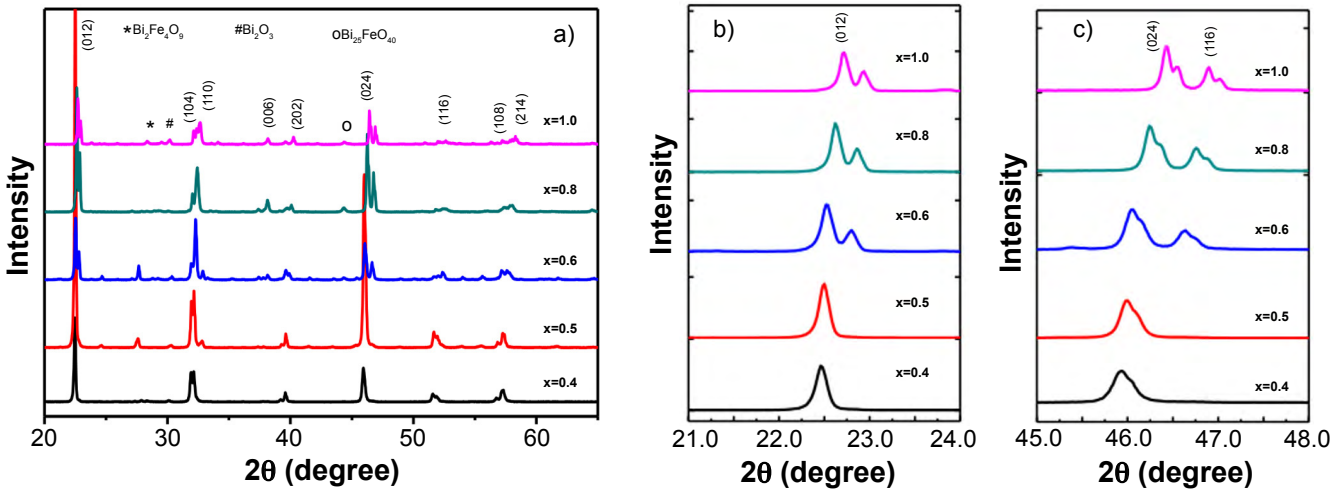

Figure 1: X-ray diffraction patterns of $BF_{1-x}C_xO_3$, x=0.4-1.0, at RT.
[Figura 1: Padrões de difração de raios X de $BF_{1-x}C_xO_3$, x=0,4-1,0, à temperatura ambiente.]

Table I - Crystal structures and lattice parameters of $BiFe_{1-x}Cr_xO_3$, x=0.4-1.0.
[Tabela I - Estruturas cristalinas e parâmetros de rede de $BiFe_{1-x}Cr_xO_3$, x=0,4-1,0.]

Sample	Structure	a (Å)	b (Å)	c (Å)	β	Cell volume (Å^3)
x=0.4	Rhombohedral	5.563	5.563	13.773	-	369.1
x=0.5	Rhombohedral	5.559	5.559	13.749	-	367.9
x=0.6	Monoclinic	9.530	5.925	9.935	107.52	535.0
x=0.8	Monoclinic	9.468	5.884	9.932	108.26	525.5
x=1.0	Monoclinic	9.435	5.891	10.070	108.19	531.7

area under the peak using Origin Pro 8 gave the value range of 2%-8% for x=0.4-1.0, respectively. For x= 0.4 and 0.5, the materials displayed a typical rhombohedral structure with R3c space group, distorted perovskite structure, and was indexed as a hexagonal unit cell. However, for x= 0.6 to 1.0, the structure changed to a monoclinic (m) C2/c symmetry. Figs. 1b and 1c show the magnified patterns at 2θ around 22.5° and 45° of the samples. The single peaks at 2θ= 22.5° and 45° of a rhombohedral structure in x=0.4 were shifted to higher 2θ giving a decrease of lattice parameter, and split gradually into two peaks, indicating that the crystal structure transformed from rhombohedral symmetry to a monoclinic symmetry when x=1 ($BiCr_{1.0}O_3$) [13]. It was clear that the material was controlled by a new structural phase for heavily doped samples. The transitional point of the structure change was identified at x=0.6 ($BiFe_{0.4}Cr_{0.6}O_3$)

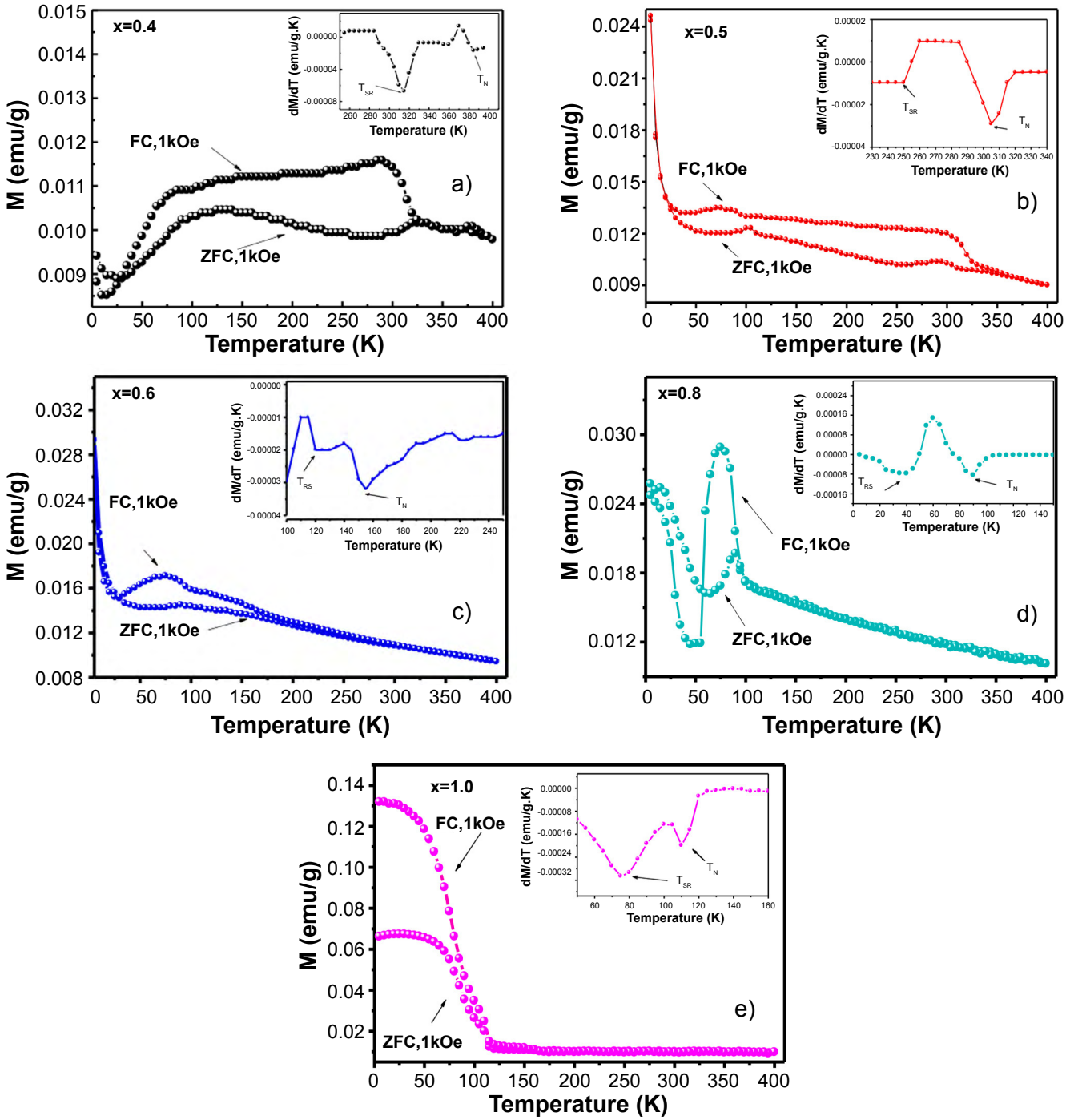

Figure 2: Variation of the magnetization (M) with temperature (T) for $BiFe_{1-x}Cr_xO_3$, x=0.4-1.0; the inset shows the plot of dM/dT curve as a function of temperature.

[Figura 2: Variação da magnetização (M) com a temperatura (T) para $BiFe_{1-x}Cr_xO_3$, x=0,4-1,0; o inserto mostra o gráfico da curva dM/dT em função da temperatura.]

Table II - Magnetic parameters of $BiFe_{1-x}Cr_xO_3$, x=0.4-1.0.
[Tabela II - Parâmetros magnéticos de $BiFe_{1-x}Cr_xO_3$, x=0,4-1,0.]

Sample	T_{SR} (K)	T_N (K)	M_{max} (emu/g)	M_r (emu/g)	H_c (kOe)
x=0.4	315	370	0.1007	0.0023	0.20
x=0.5	250	305	0.1030	0.0016	0.10
x=0.6	120	155	0.1065	0.0008	0.01
x=0.8	35	90	0.1120	0.0001	0.02
x=1.0	75	110	0.1100	0.0080	0.50

when two phases appeared. However, nearly single-phase was obtained in other samples. Also, the data showed a decrease in lattice parameters with increasing of x (Cr ions). The variation of lattice parameters with the concentration of x is illustrated in Table I.

Magnetic properties: Figs. 2a to 2e and insets show the temperature dependence of the zero-field cooled (ZFC) and field cooled (FC) magnetization (M-T) measured under a field of 1 kOe. The derivative dM/dT inset curves for BF1-xCxO3, x= 0.4, 0.5, 0.6, 0.8, and 1.0 from 230 up to 400 K are indicated. The magnetization showed Curie-Weiss like behavior above the transition temperatures. All samples revealed two magnetic transitions. The first one is the Néel temperature T_N in which the paramagnetic phase changes to the antiferromagnetic phase, and the second one has been recognized as spin-reorientation transition T_{SR} from antiferromagnetic to weak ferromagnetic ordering. The T_N and T_{SR} values were confirmed from peak positions of the FC-dM/dT plot versus T at 1 kOe, as observed in [25]. Also, by increasing Cr^{3+} ion doping, the Néel temperature T_N and spin-reorientation temperature T_{SR} shifted towards lower temperatures. The change in T_N and T_{SR} as a function of Cr concentration (x) is shown in Table II. This significant decrease in T_N and T_{SR} was probably due to the transformation of relatively heavy Fe^{3+} ions (0.645 Å) to lighter Cr^{3+} ions (0.615 Å) leading to a reduction in the concentration of Fe^{3+} ions and sublattice moments which are slightly canted along the c-axis [26, 27]. In addition, the magnitudes of magnetization increased as Cr^{3+} ion doping increased in the samples when going from heavier to lighter ions.

Room temperature magnetization hysteresis (M-H) loops of $BiFe_{1-x}Cr_xO_3$ with x= 0.4, 0.5, 0.6, 0.8, and 1.0 are shown in Fig. 3 with the inset in the field range of ±1.0 kOe. The combined plots for all the samples demonstrated a relative effect of the Cr^{3+} ion doping concentration on the magnetic properties of these samples. It is clearly seen that none of the samples exhibited saturation magnetization. This could be due to the antiferromagnetic nature of the samples. Similar behavior has been reported by several authors [28-30]. Besides, the nonzero remnant magnetization M_r and tiny magnetic hysteresis, along with the antiferromagnetic behavior as demonstrated in the inset, indicated the existence of weak ferromagnetic behavior.

The remnant magnetization M_r, maximum magnetization M_{max}, and coercivity H_c for the $BiFe_{1-x}Cr_xO_3$, x= 0.4, 0.5, 0.6,

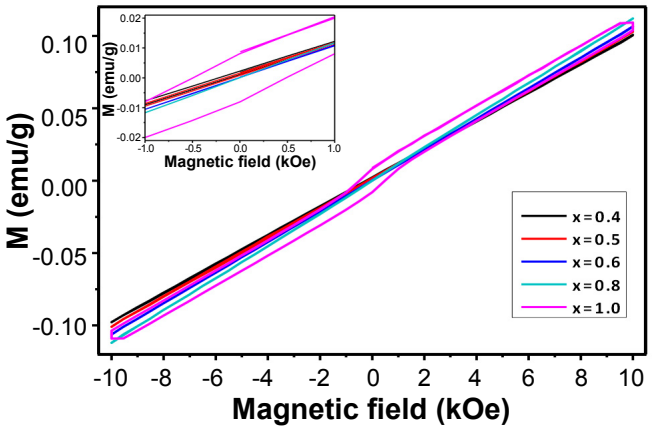

Figure 3: Magnetic hysteresis loops for $BiFe_{1-x}Cr_xO_3$, x=0.4-1.0.
[Figura 3: Laços de histerese magnética para $BiFe_{1-x}Cr_xO_3$, x=0,4-1,0.]

0.8, and 1.0 samples are listed in Table II. It was seen that the magnetization increased with the increase of Cr^{3+} ion doping in the sample. Besides, the Cr^{3+} ion doping effect was responsible for efficient ferromagnetic properties. The enhancement in magnetic properties showed by adding of Cr^{3+} ions replacing Fe^{3+} ions may be attributed to two major reasons. The first reason can be explained by the existence of the uncompensated spins in the two sublattices as a result of the different magnetic moment of Cr^{3+} ions (μ=3.87.μ_B) with regard to Fe^{3+} ions (μ=5.92.μ_B) in octahedral sites. The antiferromagnetic arrangement is associated with the direction of electron spin, where the number of spin-up is equal to the number of spin-down in the sublattices, related to the mechanism of compensation [10]. While Fe^{3+} ions were substituted by Cr^{3+} ions, the spins in the sublattices of $BiFeO_3$ were uncompensated, where the number of spin-up was not the same as the number of spin-down, resulting in a weak ferromagnetic arrangement. The second reason, the improvement of magnetic behavior with increasing the Cr^{3+} ion doping concentration in the sample may be related to the variation in the B-O-B bond angle. The substitution of Fe^{3+} ions by Cr^{3+} ions led to an increase in the canting of spins and thus enhanced the magnetization in $BiFe_{1-x}Cr_xO_3$ samples.

CONCLUSIONS

The effects of the Cr ions substitution for Fe ions of

$BiFe_{1-x}Cr_xO_3$, with x= 0.4, 0.5, 0.6, 0.8, and 1.0 on the structural and magnetic properties were studied. The structure changed from rhombohedral when x= 0.4 and 0.5 to monoclinic when x= 0.6, 0.8, and 1.0. Replacement of Fe^{3+} ions by Cr^{3+} ions significantly changed the magnetic properties of $BiFe_{1-x}Cr_xO_3$. The helical spin structure of $BiFe_{1-x}Cr_xO_3$ was improved towards a ferromagnetic structure beyond $BiCrO_3$. In addition, the Néel temperature T_N and spin-reorientation transition temperature T_{SR} shifted towards lower values with increasing x (Cr ion) from 315 K for $BiFe_{0.4}Cr_{0.6}O_3$ to 75 K for $BiCrO_3$. In conclusion, the process of substituting Cr^{3+} ions for Fe^{3+} ions of $BiFe_{1-x}Cr_xO_3$ changes the crystal structure and brings the magnetic transition temperatures T_{SR} and T_N to lower values. The M-H hysteresis loops at room temperature revealed that the doped samples $BiFe_{1-x}Cr_xO_3$ (x=0.4, 0.5, 0.6, 0.8) were antiferromagnetic while the pure $BiCrO_3$ (x=1.0) was weak ferromagnetic. The remnant magnetization and coercivity decreased starting from x= 0.4 to 0.8 and then increased in the pure $BiCrO_3$ (x=1.0) sample with enhancement in magnetic behavior with the increase of Cr doping.

ACKNOWLEDGMENTS

The author would like to express her thanks and deep gratitude to King Faisal University, College of Science, Physics Department, and the Deanship of Scientific Research for their kind support. This study was funded by the Deanship of Scientific Research (King Faisal University): proposal No. 186057.

REFERENCES

[1] M. Fiebig, Th. Lottermoser, D. Frohlich, A.V. Goltsev, R.V. Pisarev, Nature **419** (2002) 818.
[2] N. Hur, S. Park, P.A. Sharma, J.S. Ahm, S. Guha, S.W. Cheong, Nature **429** (2004) 392.
[3] T. Kimura, S. Kawamoto, I. Yamade, M. Azuma, M. Takano, Y. Tokura, Phys. Rev. B **67** (2003) 180401.
[4] S.T. Wang, H. Song, J. Mater. Sci. Mater. Electron. **29** (2018) 5566.
[5] C. Michel, K.M. Moreau, G.D. Achenbach, R. Gerson, W.J. James, Solid State Commun. **7** (1969) 701.
[6] N.A. Hill, J. Phys. Chem. B **104** (2000) 6694.
[7] B. Dhanalakshmi, K. Pratap, B. Parvatheeswara Rao, P.S.V. Subba Rao, J. Alloys Compd. **676** (2016) 193.
[8] F. Kubel, H. Schmid, Acta Crystallogr. B **46** (1990) 698.
[9] P. Fischer, M. Polemska, I. Sosnowska, M. Szymaski, J. Phys. C Solid State Phys. **13** (1980) 1931.
[10] L.G. Betancourt-Cantera, A.M. Bolarín-Miró, C.A. Cortés-Escobedo, L.E. Hernández-Cruz, F. Sánchez-De Jesús, J. Magn. Magn. Mater. **456** (2018) 381.
[11] J.T. Heron, D.G. Schlom, R. Ramesh, Appl. Phys. Rev. **1** (2014) 21303.
[12] G. Dhir, P. Uniyal, N.K. Verma, Phys. Status Solidi C **14** (2017) 1610.
[13] S. Niitaka, M. Azuma, M. Takano, E. Nishibori, M. Takata, M. Sakata, Solid State Ion. **72** (2004) 557.
[14] I. Sosnawska, W. Schafer, W. Kockelmam, K.H. Andersen, O. Troyanochuk, Appl. Phys. A **74** (2002) 1040.
[15] H. Uchida, R. Ueno, H. Nakaki, H. Funakubo, S. Koda, Jap. Appl. Phys. **44** (2005) L561.
[16] X. Qi, J. Dho, R. Tomov, M.G. Blamire, J.I. Macmanus-Driscoll, Appl. Phys. Lett. **86** (2005) 63903.
[17] S.R. Das, P. Bhattacharya, R.N.P. Choudhary, R.S. Katiyar, J. Appl. Phys. **99** (2006) 66107.
[18] R. Mazumder, A. Sen, J. Alloys Compd. **475** (2009) 577.
[19] A.J. Jorcobson, B.E.F. Fender, J. Phys. C Solid State Phys. **8** (1975) 844.
[20] S.S. Arafat, Chin. Phys. B **23** (2014) 66101.
[21] Q. Zhang, H. Zhu, H. Xu, B. Gao, J. Xiao, Y. Liang, L. Zhu, G. Zhu, Q. Xiao, J. Alloys Compd. **546** (2013) 57.
[22] F. Chang, N. Zhang, F. Yang, S. Wang, G. Song, J. Phys. D Appl. Phys. **40** (2007) 7799.
[23] V.N. Minh, N.G. Quan, J. Alloys Compd. **509** (2011) 2663.
[24] X. Qi, X. Zhang, J. Qi, H. Xu, H. Wang, Key Eng. Mater. **512-515** (2012) 1240.
[25] A.A. Belik, Sci. Technol. Adv. Mater. **16** (2015) 26003.
[26] S. Chihaoui, M. Koubaa, W. Cheilkhrouhou-Koubaa, A. Cheilkhrouhou, H. Guermazi, J. Alloys Compd. **771** (2019) 327.
[27] A. Pal, C.D. Sekhar, A. Venimadhav, P. Murugavel, J. Phys. Condens. Matter **29** (2017) 1.
[28] M.N. Hossain, M.A. Matin, M.A. Hakim, M.F. Islam, Mater. Sci. Eng. **438** (2018) 12016.
[29] A. Kumar, K. Yadav, Mater. Sci. Eng. B **176** (2011) 227.
[30] B. Wang, X. Tian, X. Song, L. Ma, S. Yu, C. Hao, K. Chen, Q. Lie, Colloid Surf. A **461** (2014) 184.
(Rec. 01/06/2019, Rev. 13/08/2019, 26/10/2019, Ac. 02/11/2019)